Acta Biomaterialia 161 (2023) 170–183

Contents lists available at ScienceDirect

Acta Biomaterialia

journal homepage: www.elsevier.com/locate/actbio

Full length article

# Global and local stiffening of *ex vivo*-perfused stented human thoracic aortas: A mock circulation study

Emmanouil Agrafiotis[a], Christian Mayer[b], Martin Grabenwöger[c], Daniel Zimpfer[b], Peter Regitnig[d], Heinrich Mächler[b], Gerhard A. Holzapfel[a,e,*]

[a] Institute of Biomechanics, Graz University of Technology, Graz, Austria
[b] Department of Cardiac Surgery, Medical University of Graz, Austria
[c] Department of Cardiovascular Surgery, Clinic Floridsdorf, Vienna, Austria
[d] Institute of Pathology, Medical University of Graz, Austria
[e] Department of Structural Engineering, Norwegian University of Science and Technology (NTNU), Trondheim, Norway

ARTICLE INFO

*Article history:*
Received 23 November 2022
Revised 25 January 2023
Accepted 20 February 2023
Available online 26 February 2023

*Keywords:*
Endovascular repair
Compliance mismatch
Aortic stiffening
Histological remodelling
Biaxial extension test

ABSTRACT

The effects of thoracic endovascular repair (TEVAR) on the biomechanical properties of aortic tissue have not been adequately studied. Understanding these features is important for the management of endograft-triggered complications of a biomechanical nature. This study aims to examine how stent-graft implantation affects the elastomechanical behavior of the aorta. Non-pathological human thoracic aortas (n= 10) were subjected to long-standing perfusion (8h) within a mock circulation loop under physiological conditions. To quantify compliance and its mismatch in the test periods without and with a stent, the aortic pressure and the proximal cyclic circumferential displacement were measured. After perfusion, biaxial tension tests (stress-stretch) were carried out to examine the stiffness profiles between non-stented and stented tissue, followed by a histological assessment. Experimental evidence shows: (i) a significant reduction in aortic distensibility after TEVAR, indicating aortic stiffening and compliance mismatch, (ii) a stiffer behavior of the stented samples compared to the non-stented samples with an earlier entry into the nonlinear part of the stress-stretch curve and (iii) strut-induced histological remodeling of the aortic wall. The biomechanical and histological comparison of the non-stented and stented aortas provides new insights into the interaction between the stent-graft and the aortic wall. The knowledge gained could refine the stent-graft design to minimize the stent-induced impacts on the aortic wall and the resulting complications.

**Statement of significance**

Stent-related cardiovascular complications occur the moment the stent-graft expands on the human aortic wall. Clinicians base their diagnosis on the anatomical morphology of CT scans while neglecting the endograft-triggered biomechanical events that compromise aortic compliance and wall mechanotransduction. Experimental replication of endovascular repair in cadaver aortas within a mock circulation loop may have a catalytic effect on biomechanical and histological findings without an ethical barrier. Demonstrating interactions between the stent and the wall can help clinicians make a broader diagnosis such as ECG-triggered oversizing and stent-graft characteristics based on patient-specific anatomical location and age. In addition, the results can be used to optimize towards more aortophilic stent grafts.



## 1. Introduction

Patients with pathologies of the thoracic aorta, including but not limited to aneurysms, dissection, and blunt aortic injury [1], benefit from endovascular repair (TEVAR) [2,3]. Local endograft-induced biomechanical events within the aortic wall might be re-

* Corresponding author at: Graz University of Technology, Institute of Biomechanics, Stremayrgasse 16-II, 8010 Graz, Austria
*E-mail address:* holzapfel@TUGraz.at (G.A. Holzapfel).

https://doi.org/10.1016/j.actbio.2023.02.028
1742-7061/

sponsible for global graft-related complications such as endoleaks, graft migration, and infolding. Insufficient understanding of these vascular ramifications makes it difficult to manage them and achieve long-term successful repair [4,5]. The clinical TEVAR success is determined by the interaction of the rigid shape-memory stent-graft and the impact on the mechanical properties of the aorta; related to blood pressure and pulse wave velocity (PWV) after the implantation as well as the stent-graft design itself [4,6].

Technological advances have resulted in self-expandable endografts that perform closer to, but fall short of, native compliance. The self-expandability feature provides radial support, limits collapse and with an oversizing of 10 – 20%, the excessive radial forces are expected to be minimized [7]. However, the biomechanical effects of stenting on global compliance and on the local tissues remain unclear. Undoubtedly, the implantation of a stiffer prosthesis compromises the elastic nature of the aorta [8] and this elastomechanical gap between the aortic wall and the stent-graft is known as the concept of 'compliance mismatch' [9].

Aortic compliance sustains dynamically the mechanical load ejected from the left ventricle in the form of pressure and volume. During systole, the aortic wall expands to relieve pressure load and accommodate half the stroke volume. This allows the wall to transition smoothly into diastole while contracting to maintain continuous blood flow [10]. This behavior is orchestrated by the three concentric and discreet zones of the aortic wall: the intima, media, and adventitia as well as their cellular contents of endothelial cells (ECs), smooth muscle cells (SMCs), and fibroblasts, respectively. The dynamic core of the aorta lies within the medial matrix, where SMCs secret elastin and collagen; arranged in elastic lamellae. The elastin content therein defines the wall elasticity, while collagen is responsible for the maximal distensibility of the wall and helps with overstretching [11,12]. In the healthy adult aorta, the number of lamellae along with their thickness depends on the blood pressure-volume interplay and age [13]. With age, the SMCs decrease, the elastic fibers are fragmented, while the collagen fibers increase [12,14]. Therefore, the aorta stiffens naturally and consequently compliance reduces, as described in [15,16]. Another age-related stiffening process concerns diffuse intimal fibrosis. Gradually, collagen deposition transforms a denser fiber network in the intima, resulting in a thicker intima [17] and presumably a stiffer aortic wall.

The physiological hemodynamic interaction of blood pressure and aortic wall maintains canonical pathways and matrix integrity [18]. However, the deployment of a stent-graft against the aortic wall compromises the lumen-wall interaction and physiological layer-to-layer communication. The lumen-wall interface disrupts the cyclic hemodynamic stimulus to the SMCs required to maintain wall homeostasis. From a mechanobiological point of view, the stent-induced local wall deformation might influence the EC-SMC crosstalk and its phenotype, and finally induce extracellular matrix (ECM) remodeling. The stented aorta encounters altered tensile stress, shear stress, and SMCs show less contraction [19]. Non-physiological mechanotransduction can express matrix proteases (MMPs) or dysfunctional collagen. Ergo, the aortic wall stiffens due to elastin loss (e.g., matrix proteolysis or elastin rupture) and can trigger collagen overexpression after stent-induced vessel injury [20,21].

In addition to the pathophysiological stiffening, the aorta itself adopts the global compliance of the stent-graft; leading to a compliance mismatch. The degree of mismatch is inextricably linked to the oversizing of the stent-graft. Clinically, an oversizing of 10 – 30% is targeted, but consensus on accuracy is lacking. This range appears to be beneficial due to adequate proximal sealing and in combination with self-expandable grafts to achieve the desired radial force. It should be noted that there is no standard diagnostic procedure (i.e. association of systole-diastole scanning, hypertension, blood flow characteristics, etc.) and the oversizing decision based on patient-specific clinical screening is still an estimate [22,23]. Another concern arises from the unknown elastin content, which varies in each patient and poses a risk during implantation. Despite the benefits of some oversizing, it can increase the compliance gap and influence the elastomechanical performance of the aorta. Therefore, it can be assumed that from a biomechanical point of view, there are two stent-graft manifestations towards aortic stiffening:

(i) *Global effect:* Radial deployment of the stent-graft overstretches the aortic wall and the fibers therein both in the longitudinal and circumferential direction. Thus, wall distensibility could reach its dilatation threshold while the cyclic pressure wave helps to overextend the wall beyond this point. Permanent overstretching of the wall can progressively lead to elastin loss, which in turn reduces aortic compliance. These events promote vascular stiffness and force the wall to expand uniformly. Continuous uniform overstretching can also damage the collagen fibers [11,20]. As a consequence, the wall shifts to reduced elasticity that extends along the length of the stent-graft. The extent of its effect depends on the degree of oversizing and whether the stent-graft is implanted near the aortic arch; the latter contributes significantly (50%) to the total arterial compliance [24].

(ii) *Local effect:* When overstretched, the stent struts indent the intimal surface, possibly the medial layer, and increase loading above the physiological threshold (i.e., supraphysiological loading). At the cellular level, this is perceived as damage and drives mechanobiological cascades both for the ECs (intima) and SMCs (media). Subsequently, SMCs differentiate into a synthetic phenotype and deposit new collagen fibers in the media, resulting in wall stiffness [25]. The depth of the indentation depends on the stent-graft oversizing and the designed strut size; the bigger these are, the deeper the indentation in the wall. Strut-induced damage promotes neointimal hyperplasia and medial thickness. Collagen fibers surrounding the strut are inevitably compressed (also stretched) and the amount of elastin is significantly less than in the uncompressed area, as reported in a porcine study [26], and it could be relevant for human tissue. These biomechanical conditions occur locally where struts are present.

Assuming these assumptions are correct, cyclic supraphysiological loading against the aortic wall could imply overstretching, local injury, and eventually wall stiffness. The potent manifestations mentioned above are more pronounced proximally, where the stent-graft is deployed and compliance is highest. The greatest radial forces and their effect on the wall can be expected at the contact point. Therefore, the focus of interest is on the proximal area, which is prone to stent-related complications [5].

Aortic compliance is determined by biomechanical events [27,28] and to understand this, the post-TEVAR results need to be accelerated. To the author's knowledge, these biomechanical manifestations have not yet been reported for human tissue. This can be achieved with an in vitro environment that simulates the hemodynamics of the aorta, such as a mock circulation loop (MCL) specifically designed to test stented arteries [29]. To date, compliance mismatch and post-TEVAR stiffness results have been studied in human autopsies or animal tissues and often neglect the factor of oversizing.

Numerous clinical studies have reported compliance mismatch using PWV, the gold standard indicator of aortic stiffness [30–33]. Youssef *et al.* [33] conducted a comparative study by reporting increased PWV in the TEVAR group, which was oversized by 10 to 20% compared to the control group, indicating increased aortic stiffness. In another clinical study, increased PWV was reported

post-TEVAR with the stent-graft being responsible for discounting the pulsatile waves [31]. The PWV-based study [34] reported increased aortic stiffness in 40 patients undergoing TEVAR, but the extent of oversizing is not mentioned. In a systematic review, clinicians use patient databases to argue the extent of oversizing [23]. Although there was no clear result regarding oversizing, the authors concluded that oversizing should remain below 30%.

In a study consistent with this conclusion, pigs underwent TEVAR in four different oversized groups, where the authors recommended an oversize below 30% [26]. Strain strength findings were compared to a group without a stent. Elasticity decreased significantly in the stented group and continued to decrease with each subsequent oversizing. Recently, in vitro experiments were performed with 10% oversized porcine aortas in an MCL [35]. By measuring the PWV in a variety of stent-grafts, the stiffness of the aorta increases after deployment [36]. Moreover, the magnitude of stiffness was correlated with the stent-graft length; the longer it is, the more pronounced the induced vascular effects should be [35]. The same group employed an MCL to perform TEVAR experiments in porcine aortic tissue under constant pressure. They reported a two-fold stiffening post-TEVAR, a strain mismatch in the longitudinal direction [37], and the radial direction [38]. The elastomechanical properties of human aortas in an MCL under cyclic perfusion have been studied [15]. The aim was to compare changes in diameter-based compliance between aortic grafts [39,40] and non-stented descending aortas correlating stiffness variations with age. A significant compliance difference in material characterization between the non-stented human aortic wall and the graft was highlighted [15].

While results from porcine studies provide insight into aspects of stenting, they cannot be directly extrapolated to human. Of importance and relevance is the experimental investigation of stented human aortas to accelerate post-TEVAR outcomes and to assist the development of more aortophilic endovascular prostheses. This study aims to replicate the TEVAR procedure in vitro and investigate the biomechanical effects of the stent-graft in relation to oversizing. Stenting of pathological aortas may not alter the already compromised elastomechanical properties of the tissue. Hence, to quantify the stent-induced loss of elasticity, stented non-diseased human aortas of different ages and oversizes are dynamically perfused in an MCL under a healthy state. By comparing the proximal tissues without and with a stent, this study elaborates: (i) aortic compliance of pre- and post-stented periods, (ii) biomechanical analysis using strength and stiffness profiles, and (iii) histological observations of the two conditions.

## 2. Materials and methods

### 2.1. Preparation of aortas

Non-diseased thoracic aortas of human cadavers ($n = 9$), in addition to age-relevant calcification, aged 38 to 81 years (mean age $62.6 \pm 11.2$ years) were obtained from the Diagnostic and Research Institute of Pathology, Medical University of Graz, Austria. The investigated specimens were explanted and collected during routine clinical autopsies, and the morphology of the aortic arch was respected. The use of donor specimens was approved by the Ethics Committee at the Medical University of Graz ($32 - 451$ ex 19/20). Autopsy protocol dictates that bodies be refrigerated after death. To ensure tissue integrity, autopsies showing a cold ischemic time longer than 24 hours were not accepted for this study. The cold ischemic time refers to the interim time between the declaration of death and tissue recovery. Table 1 summarizes the specifications of all donors, including cold ischemic times, aortic and stent-graft dimensions. Within two hours of autopsy, specimens were tested in the MCL to minimize the progression of autolysis and degradation of tissue integrity. After removal of the periaortic adipose tissue, the aortic specimens were stored in transplant containers and transported to the test site at 4°C in a phosphate-buffered saline (PBS) solution (0.9% w/v of NaCl). Surgical closure of the branches was performed prior to testing to prevent leakages during testing.

### 2.2. Mock circulation loop

For this study, a custom MCL was developed to test stented thoracic aortas (Fig. 1). Briefly, the MCL consists of a simulated left ventricle to provide pulsatility, pressure, and flow. A unique active compliance chamber was introduced into the arterial segment to simulate the Windkessel effect. Its movement was tuned to reform the cyclic pulse pressure of the arterial segment and equalize it with the programmed reference pressure. The nonlinear displacement of the chamber ensures the accuracy of the aortic pressure ($p_{\text{aorta}}$) and the Windkessel effect. For a detailed description see Agrafiotis *et al.* [29]. A customized transparent testing unit with a heated coil was designed to submerse whole aortas in a 37°C liquid bath. The inlet and outlet of the testing unit are designed in such a way that the aorta maintains its natural arch-shaped position when mounted. A liquid reservoir of 4.5 L was placed further downstream to supply the circulation. A heating coil was placed inside to pre-heat the liquid to 37°C prior to testing. The two coils are operated by two ECO laboratory thermostats (LAUDA GmbH & Co. KG, Lauda-Königshofen, Germany). Real-time temperature was measured with a digital thermometer. Both the circulatory liquid and the liquid of the testing unit were a blood-analogous solution of glycerin–d$H_2O$ 50.6% v/v (pH 7.4) (Carl Roth GmbH, Karlsruhe, Germany), to achieve equal rheological properties [41]. The specimens were mounted in adaptors with a diameter similar to the inner diameter (ID) of the specimen. Diameter variations of the adaptors were 3D-printed to accommodate the size of each specimen for the ascending and descending IDs of the aorta. The specimens were attached to the adaptors with cable binders.

All elements of the MCL were controlled and monitored by the control unit. The stroke volume is generated by the defined displacement of the simulated left ventricle used as a reference volume. Three closed flasks were installed perpendicular to the flow to help remove air from the circulation. A roller pump (120U, Watson-Marlow GmbH, Vienna, Austria) was used to recirculate the liquid from the testing unit to the reservoir in case the aorta leaked during perfusion (something that naturally blood prevents). Pressure sensors (BSP0052, Balluff GmbH, Filderstadt, Germany) with a measuring range of $-750$ to 1500 mmHg and accuracy of $\pm 0.5\%$ were placed at the inlet of the testing unit ($p_{\text{aorta}}$), and the outlet of the testing unit ($p_{\text{cc}}$) where the descending aorta meets the compliance chamber. To compare aortic compliance, the cyclic distention of the pre- and post-stented aorta was tracked. This was possible by marking the proximal convexity and the concavity in the circumferential direction with permanent markers. The cyclic circumferential displacement ($d_{\text{circ}}$), i.e. the distance between the two markers, was measured using a camera (UI-3070CP, IDS, Obersulm, Germany) integrated into a videoextensometer (VE) (Laser Speckle Extensometer 2.23.3.0 Messphysik Materials Testing, Fürstenfeld, Austria) with a resolution of $\pm 0.15\,\mu$m and a sample rate of 120 Hz. Prior to each measurement, the distance of the VE markers was calibrated with a grip scale at 1 mm.

#### 2.2.1. Preconditioning

The hemodynamic profile used for this study was the healthy one: 60 beats per minute (bpm), a systolic pressure $p_{\text{aorta}}$ of 120 mmHg and a diastolic pressure of 80 mmHg. The stroke volume at a healthy state is 70 mL, however, the perfused volume reaching the descending aorta is 45 mL because the difference is distributed in previous vessels [42]. For this reason, the simulated

**Table 1**
Donor specification, cold ischemic time, proximal pre- and post-stented lumen diameter, stent-graft dimension, and percentage of oversizing are described.

| Donor | D1 | D2 | D3 | D4 | D5 | D6 | D7 | D8 | D9 | D10 (Histology) |
|---|---|---|---|---|---|---|---|---|---|---|
| Age (years) | 60 | 56 | 65 | 81 | 62 | 38 | 61 | 79 | 62 | 64 |
| Gender | F | F | M | M | M | M | M | M | F | M |
| Cold ischemic time (hours) | 8 | 20 | 15 | 6 | 10 | 16 | 22 | 10 | 22 | 23 |
| Stent-graft length (mm) | 80 | 80 | 130 | 130 | 170 | 130 | 130 | 130 | 130 | 130 |
| Aortic outer diameter (mm) | 28.6 | 30.0 | 25.1 | 27.4 | 27.3 | 25.0 | 29.0 | 30.2 | 29.3 | 28.6 |
| Mean wall thickness (mm) | 2.1 | 1.7 | 2.2 | 2.2 | 1.4 | 1.8 | 2.1 | 2.3 | 2.2 | 1.9 |
| Pre-stented lumen diameter (mm) | 24.4 | 26.6 | 20.7 | 23.0 | 24.5 | 21.4 | 24.8 | 25.6 | 24.9 | 24.7 |
| Stent-graft diameter (mm) | 28 | 30 | 26 | 26 | 30 | 24 | 26 | 26 | 26 | 30 |
| Post-stented lumen diameter (mm) | 25.3 | 27.4 | 21.8 | 25.6 | 25.8 | 24.3 | 26.3 | 26.7 | 26.6 | 25.8 |
| Oversizing | 15% | 10% | 25% | 15% | 20% | 10% | 10% | 5% | 10% | 20% |

D# = donor; F = female; M = male

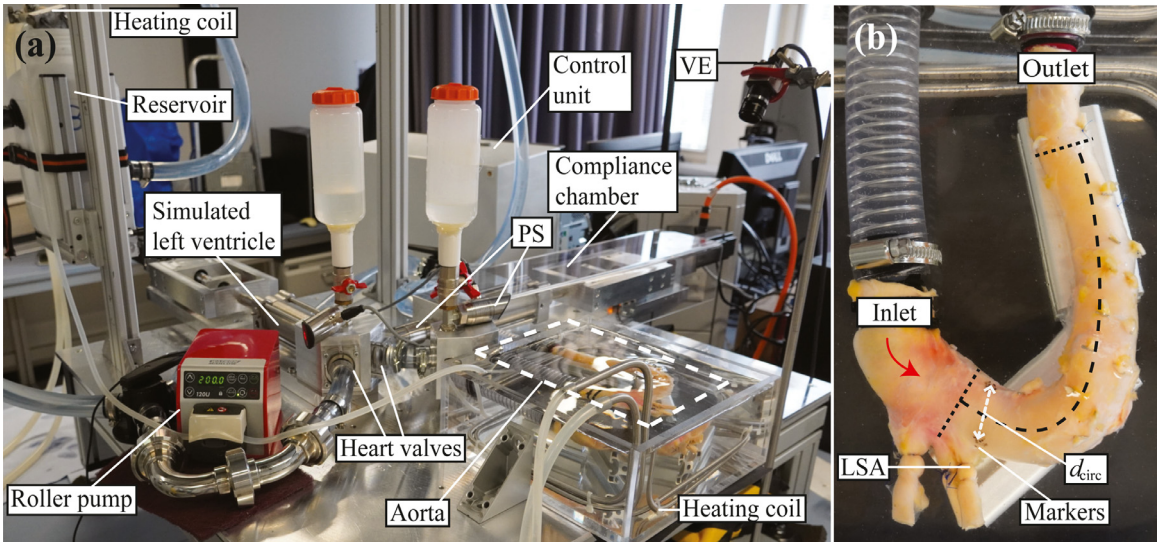


**Fig. 1.** (a) Overview of the MCL and its components with a stented aorta; (b) stented aorta in arch-shaped position during perfusion mounted in the MCL. Inlet and outlet, LSA, and proximal markers ($d_{circ}$) at the concavity and convexity are indicated. The area of interest where the stent-graft will be implanted is shown with dashed curves. The red arrow indicates the flow direction. MCL = mock circulation loop; LSA = left subclavian artery; PS = pressure sensor; VE = videoextensometer; $d_{circ}$ = proximal displacement between the markers. (For interpretation of the references to colour in this figure legend, the reader is referred to the web version of this article.)

left ventricle was set to pump 45 mL. Prior to the TEVAR procedure, the aorta underwent a preconditioning phase to adapt to the new loading environment and achieve a mechanically repetitive response. First, the aorta was mounted into the testing unit in an arch-shaped position, as presented in Fig. 1(b). The MCL was filled with glycerin-d$H_2O$ 50.6% v/v (pH 7.4, 37° C) to perfuse the specimen without filling the testing unit. This helped visualize residual leakages of the aortic wall and seal it with metal surgical clips or sutures. The aorta was then immersed in glycerin by filling the testing unit and the specimen was perfused with glycerin until the diastolic pressure of 80 mmHg was reached. Initially, the aorta was suspended naturally due to inherent residual stresses. Over time, this effect gradually diminished, and the exact moment of free hanging was unknown. To prevent hanging against gravity, two stands were preemptively placed under the aorta. However, it was observed that the aorta floated in the solution during perfusion. For preconditioning, each specimen is tested in the healthy scenario for 5 – 10 minutes depending on the natural elasticity of the tissue and the age of the donor. The mark for the end of the preconditioning phase was when the amplitude of 80 – 120 mmHg and the reference pressure waveform were repeatedly achieved. After the tissue was preconditioned, the reproduced $p_{aorta}$, $p_{cc}$, and $d_{circ}$ of 60 cycles were recorded for the non-stented (NS) measurement.

*2.2.2. Stent-graft implantation*

The area of interest was the proximal area where the stent-graft was deployed. After the NS measurement, the circulation was emptied, and the specimen was unmounted from the testing unit and prepared for the TEVAR procedure. The specimen was immersed in the testing unit filled with glycerin (37°C) to deploy the stent-graft. The TEVAR procedure was performed outside of the MCL for two reasons: (i) to ensure proper placement of the stent-graft since angiography was not available on-site, and (ii) not to interfere with the pulsatile circulation of the MCL by opening it to the atmosphere. A polyester thoracic stent-graft was selected for this study (E-vita Thoracic$^{3G}$, Jotec, Hechingen, Germany). The stent-graft is flexible and self-expandable with Nitinol (NiTi alloy) struts sewn in a 'zigzag' pattern. As no visualization tool was available on site, the oversizing for each donor was based on the pre-stented outer diameter (OD) of the aortas. The lumen was pressurized manually via the interface at a mean aortic pressure of $p_{aorta}^{mean} = 95 - 100$ mmHg in the MCL and the ODs were measured with a digital caliper. The oversizing was calculated using the recommended formula [43]

$$SG\varnothing = Lumen\varnothing + OS\%, \quad Lumen\varnothing = OD - 2\bar{T}, \tag{1}$$

where $\bar{T}$ is the mean wall thickness, $OS\%$ is the desired oversizing percentage, $SG\varnothing$ is the stent-graft diameter and $Lumen\varnothing$ is the lumen diameter.

The stent-graft delivery system consisted of a sheath enclosing the stent-graft and control handler. The sheath was inserted retrogradely into the aortic lumen under direct vision and positioned at the ostium of the left subclavian artery (LSA). By intermittently pressing the lever on the handler, the proximal bare struts were protruding from the sheath but were not yet deployed; crimped within a tip. Further sheath retraction was followed until the first three zigzag lines of struts were released. The bare struts are then deployed by releasing the tip while observing the aortic wall directly. The remainder of the stent graft was gradually deployed and then the delivery system was removed from the lumen. A detailed description of the stent-graft and its delivery system can be found in [44].

#### 2.2.3. Perfusion of stented aortas

After the stent-graft was implanted, the aorta was mounted to the MCL adaptors in an arch-shaped position. The MCL was gradually filled with glycerin until the arterial segment reached $p_{\text{aorta}} =$ 80 mmHg, at which point the aorta adopted its natural diastolic diameter. Subsequently, the testing unit was filled with glycerin solution until the aorta was covered to provide a physiological environment. this is followed by a gradually controlled pulsation from 10 to 60 bpm to ensure circulation is vented and the tissue is sealed. The MCL then simulated the healthy hemodynamic profile: 60 bpm and an aortic pressure amplitude of 80 − 120 mmHg. The duration of the stented perfusion was eight hours to simulate the in vivo loading scenario that the aortic wall is exposed to after TEVAR. Preliminary tests were conducted to determine the testing duration of the aortas in the MCL based on physical characteristics. Stented measurements (S1-S4) were performed every two hours. During the measurements, the pressure of ascending ($p_{\text{aorta}}$) and descending ($p_{\text{cc}}$) portions as well as $d_{\text{circ}}$ between the markers were recorded for 60 cycles. During perfusion, the lumen and the periaortic temperature were maintained at $37 \pm 0.5$°C.

### 2.3. Compliance mismatch

The elastomechanical gap between the non-stented and stented experimental periods was described as the cyclic relationship of $p_{\text{aorta}}$ vs $d_{\text{circ}}$. To examine the difference in the elasticity of the aorta in the non-stented and the stented period, the NS measurement was compared against the S1-S4 measurements. The reproduced pressure values $p_{\text{aorta}}$ at the inlet of the testing unit were measured by the pressure sensor. By tracking the markers at the proximal concave and convex, the cyclic circumferential displacement $d_{\text{circ}}$ was recorded. The dynamic relationship of $p_{\text{aorta}}$ vs $d_{\text{circ}}$ was synchronized by matching the systolic peaks of $p_{\text{aorta}}$ and $d_{\text{circ}}$ waveforms (Fig. 2(a),(i)). This was necessary because the pressure sensor was located at the inlet of the ascending aorta, whereas the camera was tracking the movement of the markers distally to the LSA. However, the $p_{\text{cc}}$ values that were measured downstream in the descending part are basically identical (Fig. 2(a),(ii)) due to the Windkessel effect imposed by the active compliance chamber and reassure that $p^{\text{mean}}_{\text{aorta}}$ remains the same. To quantify the compliance mismatch in the transition from the non-stented to the stented state, the maximum displacement thresholds of $d^{\text{NS}}_{\text{max}}$ and $d^{\text{S}}_{\text{max}}$ were outlined in Fig. 2(b), respectively. The loss of distensibility $D_{\text{loss}}$ was calculated via the relation

$$D_{\text{loss}} = 100\,\frac{d^{\text{NS}}_{\text{max}} - d^{\text{S}}_{\text{max}}}{d^{\text{NS}}_{\text{max}}}\%, \tag{2}$$

and correlated with the respective stent-graft oversizing (see Table 2).

The hysteresis loops in Fig. 2(b)-(d) are the average of 60 cardiac cycles for the measurements NS and S1-S4. The accuracy of the measured $p_{\text{aorta}}$ and $p_{\text{cc}}$ is illustrated in Fig. 2(a),(ii) in the form of a cycle as the mean pressure of $n = 20$ cycles for the non-stented (red waveforms) and the stented (blue waveforms) periods. Representative measured waveforms of 10 cycles of $d_{\text{circ}}$ are demonstrated in Fig. 2(a),(ii) and are related to the S2 measurement of D6. Measured $d_{\text{circ}}$ waveforms were filtered in MATLAB (R2020a, The MathWorks Inc., Natick, USA) to show the hysteresis loops. The filtered waveforms were stacked over one cycle in Fig. 2(a),(i) and synchronized with the systolic pressure peaks. Both periods show a low $\sigma = 0.20$ mmHg with a reproduced measurement every millisecond. The precise autoregulatory mechanism for pressure control is described in detail in [29].

**Table 2**
Experimental data from distensibility group i) and ii) correlating the mean pressure ($p^{\text{NS–S}}_{\text{mean}}$), the maximum circumferential displacement between the markers ($d^{\text{max}}_{\text{circ}}$), maximum systolic displacement for non-stented ($d^{\text{NS}}_{\text{max}}$) and stented ($d^{\text{S}}_{\text{max}}$) periods, oversizing, and the loss of distensibility ($D_{\text{loss}}$) between systolic $d^{\text{NS}}_{\text{max}}$ and $d^{\text{S}}_{\text{max}}$.

| Group (i) | Age (yrs) | $p^{\text{NS–S}}_{\text{mean}} \pm$ SD (mmHg) | $d^{\text{max}}_{\text{circ}}$ (mm) | $d^{\text{NS}}_{\text{max}}$ (mm) | $d^{\text{S}}_{\text{max}} \pm$ SD (mm)±(mm) | OS (%) | $D_{\text{loss}}$ (%) |
|---|---|---|---|---|---|---|---|
| D1 | 60 | $95 \pm 0.3$ | 1.88 | 0.80 | $0.60 \pm 0.13$ | 15 | 25 |
| D2 | 56 | $97 \pm 0.6$ | 3.28 | 1.65 | $1.20 \pm 0.15$ | 10 | 27 |
| D3 | 65 | $94 \pm 0.3$ | 3.50 | 1.87 | $0.57 \pm 0.12$ | 25 | 69 |
| D4 | 81 | $93 \pm 0.7$ | 2.42 | 0.98 | $0.54 \pm 0.05$ | 15 | 45 |
| (ii) | | | | | | | |
| D5 | 62 | $94 \pm 0.7$ | 0.38 | 0.18 | $0.02 \pm 0.007$ | 20 | 88 |
| D6 | 38 | $94 \pm 0.8$ | 0.64 | 0.29 | $0.16 \pm 0.020$ | 10 | 45 |
| D7 | 61 | $93 \pm 0.3$ | 0.27 | 0.16 | $0.07 \pm 0.002$ | 10 | 57 |
| D8 | 79 | $92 \pm 0.6$ | 0.28 | 0.16 | $0.10 \pm 0.001$ | 5 | 38 |
| D9 | 62 | $94 \pm 0.5$ | 0.26 | 0.15 | $0.06 \pm 0.003$ | 10 | 60 |

(D#) = donor; $p^{\text{NS/S}}_{\text{mean}}$ = mean aortic pressure of non-stented/stented; $d^{\text{max}}_{\text{circ}}$ = maximum displacement between the markers; $d^{\text{NS}}_{\text{max}}$ = non-stented maximum systolic displacement; $d^{\text{S}}_{\text{max}}$ = stented maximum systolic displacement; SD = standard deviation; OS = oversizing; $D_{\text{loss}}$ = systolic distensibility loss due to stenting.

### 2.4. Biaxial tensile tests

After the long-standing stented perfusion, the loose connective tissue and adipose tissue were removed. The tissue was dissected along the longitudinal convexity site until the specimen was cut open. The stent-graft was then carefully detached from the aortic wall and the proximal aortic wall was dissected into smaller samples for mechanical testing. Tissue samples were taken from the proximal non-stented aorta and stented aorta. The number of samples of each specimen varied based on the condition of the tissue. Areas with atherosclerosis and vessel branches were excluded. The samples were then stored in PBS in a freezer at −24°C for a short time (maximum = 7 days) until testing. Prior to testing, all samples were thawed overnight at 4°C.

In order to investigate the tissue integrity post-TEVAR from a biomechanical point of view, a comparative analysis between the non-stented and the stented tissue samples was carried out. Stented samples were taken from the strut-indented zone. In particular, the samples were tested equibiaxially to investigate the stiffness and strength profile between non-stented and stented tissue. In this study, all three layers of aortic tissue were included. Prior to testing, the initial thickness $T$ was measured optically with VE. Square samples of $10 \times 10$ mm were extracted from the area of interest. The samples were then marked with black powder on the intimal surface for video tracking and then mounted in a biaxial testing device via hooked surgical sutures. The samples were immersed in a PBS bath at 37°C using the detailed biaxial device protocol described in [45]. Briefly, a stretch-driven protocol ($\lambda$) was used with a step of 0.05 stretch until rupture. For every stretch, a variety of stretch ratios were conducted: $\lambda_{\text{long}} : \lambda_{\text{circ}} = 1:1, 1:0.75, 0.75:1, 1:0.5, 0.5:1$, where $\lambda_{\text{long}}$ indicates the stretch in the longitudinal direction while $\lambda_{\text{circ}}$ the stretch in the circumferential direction. With every shift to the next stretch

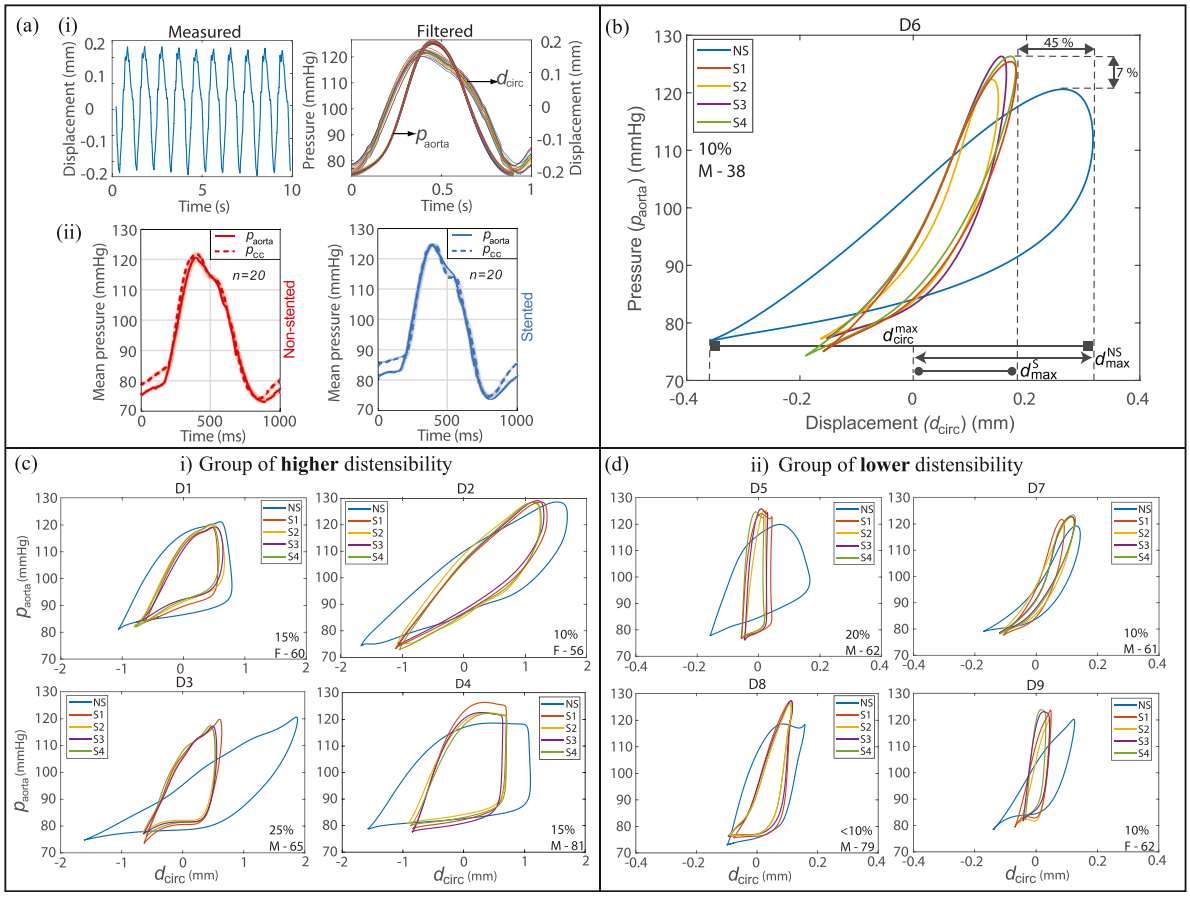


**Fig. 2.** (a): (i) Representative measured 10 cycles of $d_{circ}$ and filtered values of $p_{aorta}$ and $d_{circ}$ for the S2 measurement of D6; (ii) mean pressure waveforms (from 20 cycles) of the ascending aorta for the non-stented (red) and stented period (blue). (b) Analytical graph for a significantly younger patient (D6). The blue loop denotes the compliance of the aorta in the non-stented period labeled NS. The remaining loops indicate the compliance after implantation of the stent-graft labeled S1-S4. $d_{circ}^{max}$ indicates the maximum circumferential displacement between the markers during the cardiac cycle. $d_{max}^{NS}$ denotes the maximum systolic displacement for the non-stented period, $d_{max}^{S}$ is the maximum systolic displacement in the stented period. (c) Proximal hysteresis loops of pressure $p_{aorta}$ vs displacement $d_{circ}$ of group i), donors (D#) with higher distensibility and (d) of group ii), with lower distensibility. NS = non-stented measurement; S = stented measurement; $d_{max}^{NS}$ = non-stented maximum systolic displacement; $d_{max}^{S}$ = stented maximum systolic displacement; $d_{circ}$ = circumferential displacement; $p_{aorta}$ = aortic pressure; the labeling %, M/F, number in (b), (c) and (d) means the amount of oversizing, gender (male/female), and age in years of the donor, respectively. (For interpretation of the references to colour in this figure legend, the reader is referred to the web version of this article.)

level, the samples underwent four cycles of preconditioning when a repetitive response was reached and the subsequent fifth cycle was the actual measurement. A quasi-static loading rate of 3 mm $min^{-1}$ was applied. The Cauchy stresses were then calculated by

$$\sigma_{long} = \frac{f_1 + f_2}{2WT}\lambda_{long} \quad \text{and} \quad \sigma_{circ} = \frac{f_3 + f_4}{2WT}\lambda_{circ}, \tag{3}$$

where $f_1$, $f_2$, $f_3$ and $f_4$ are the measured forces at every load cell and $\lambda_{long/circ} = l/L$ the stretches in the longitudinal and circumferential direction, calculated with the distances from the reference configuration $L$ and the deformed configuration $l$, while $W$ represents the width and $T$ the thickness of the sample.

### 2.5. Histology

To perform histological fixation, a separate aorta (case D10) was oversized by 20% and perfused in the MCL according to the above protocol. In order to visualize the strut indentation (SI) on the lumen wall, post-perfusion of the stented aorta had to be fixed with the stent-graft immersed into formaldehyde 4% solution (ROTI® Histofix, Carl Roth, Karlsruhe, Germany) where it remained overnight. After fixation, the aorta was dissected along the convexity, cut open, and the stent-graft was removed. NS and S specimens were dehydrated in a series of 70 – 100% ethanol followed by paraffin embedding. Then, Hematoxylin and Eosin (H&E) staining and Elastica van Gieson (EvG) were performed for ECs and SMCs nuclei identification, and elastic and collagen fibers, respectively. The histological slides were scanned in the 3DHISTECH P1000 slide scanner (3DHISTECH Ltd., Budapest, Hungary) and then evaluated with the 3DHISTECH CaseViewer software. Then histological images were processed digitally with Fiji [46].

## 3. Results

### 3.1. Proximal dynamic compliance

The plots in Fig. 2(c),(d) show the global dynamic compliance at the proximal site of eight different donors plotted as hysteresis loops from $p_{aorta} - d_{circ}$ in the physiological pressure range. The loops reveal the amount of stiffening added by the stent-graft, presented as a comparative analysis of the non-stented (NS) and the stented (S1-S4) period. S1-S4 loops were recorded two hours apart and it can be seen that the post-stented behavior is altered significantly from S1 and remained the same thereafter. As each specimen exhibits a unique viscoelastic behavior, all donor loops are presented and classified into two groups of viscoelastic-

ity: i) the higher dynamic elasticity (D1-D4) with a greater range of $d_{\text{circ}}^{\text{max}} = 3.50$ mm (plot D3) and ii) the lower dynamic elasticity (D5-D9) with a lower range, i.e. $d_{\text{circ}}^{\text{max}} = 0.64$ mm (plot D6), based on cyclic distensibility. In both groups, the $p_{\text{aorta}}$ ranged within physiological limits of 75 to 128 mmHg. The MCL itself reproduces accurately the reference pressure amplitude of 80 − 120 mmHg. Therefore, due to the congenital stiffness of the aorta, small deviations occur.

### 3.2. Compliance mismatch – Oversizing

Fig. 2 (b) stands as a unique case of a younger donor (D6) of group ii) with the most pronounced $d_{\text{circ}}^{\text{max}} = 0.64$ mm and as a representative plot for the analysis of the loops. The values for the maximum non-stented and stented samples are $d_{\text{max}}^{\text{NS}} = 0.29$ mm and $d_{\text{max}}^{\text{S}} = 0.16 \pm 0.02$ mm, respectively, mark the systolic distensible limits. After stent-graft implantation, the systolic border suffers a 45% drop. The area within the loop denotes the amount of energy stored during the cardiac cycle (i.e., the distensibility of the aorta). This area is significantly reduced after implantation of the stent graft, which means that the loss of elasticity is accompanied by a loss of capacity of the stored energy [47]. In addition, D6 is a representative plot in terms of oversizing. In this case, the oversizing performed was 10%. From the age and the resulting loops, it can be deduced that D6 is the more elastic aorta of group ii). However, its post-stented elastomechanical behavior underlines the influence of the stent-graft on the elastic behavior. A systolic pressure increase of 7% is noticeable from $p_{\text{aorta}}^{\text{sys}} = 120$ mmHg to $p_{\text{aorta}}^{\text{sys}} = 127$ mmHg in the stented period, but still within physiological limits. This is thought to be caused by the closure of the aortic valve in the MCL, resulting in a restricted volumetric segment of the aorta. When the stented aortic segment stiffens, some of the energy previously stored in the aortic wall from distention is converted into an increase in pressure. It can be assumed that in vitro this behavior is length-dependent since D4-D9 were implanted with a stent-length of 130 mm, with the exception of D5 (170 mm) and show similar behavior. In contrast to D1-D2 which own a stent-length of 80 mm this is not the case. It should be noted that age and oversize factors play an indirect role in this transition.

Based on the above analysis, Table 2 correlates the experimental results of Fig. 2(c),(d) for group i) and ii) on proximal dynamic compliance and its loss due to oversizing. The correlation shows the direct influence of the stent-graft and possibly extends to the oversizing of $d_{\text{max}}^{\text{NS}}$ and the loss of compliance within the first hours of perfusion after TEVAR. It is noticeable that this loss depends on the oversizing; the greater the oversizing (e.g., D3), the more pronounced the loss of distensibility, denoted as $D_{\text{loss}}$. In particular, cases D3, D4 of the higher elasticity group show that $D_{\text{loss}}$ is greater due to the oversizing of 25% and 15%. Despite these observations, one must keep the small sample size in mind and carefully extract the information on whether the losses are directly attributable to the oversizing factor, age, and/or the stent-graft itself.

### 3.3. Proximal mechanical response

The local mechanical behavior of the proximal site between the non-stented (NS) and stented (S) region for each donor is shown in Fig. 3. To visualize the NS-S areas as well as the stretching directions, the reader should refer to Fig. 4(a). Non-stented samples were taken from the non-atherosclerotic NS area and stented samples were extracted from the strut patterns of the S area. The nonlinear stress-stretch curves loaded biaxially in the longitudinal and the circumferential direction are the mean curves of non-stented (black curve) against stented (red curve) samples. The non-stented curves describe the behavior of the natural aortic tissue and are to be seen as control behavior versus the stented tissue, reflecting the stent-induced altered behavior. If the stented curve shows behavior above the non-stented curve, the response is considered to be stiffening. In contrast, a stented behavior below the non-stented curve is called softening [48]. Both areas are plotted relative to the maximum stretch level before rupture to illustrate the extent to which the stent-graft has mechanically affected the tissue. The SD of the different samples is represented by the semi-transparent region. Only the loading path is chosen because the unloading path has no visible softening. The term strength in the present equibiaxial series is understood as the maximum withstanding stretch-driven stress before permanent deformation. This enables strength comparisons of the two states within the elastic phase. Depending on the nature of the tissue, the number of samples per area varied ($n = 3 - 6$; see Table 3).

The stress–stretch responses of all donors are classified into groups of higher (i) and lower (ii) elasticity (Fig. 3) based on the stented response. The stented tissue in group i) shows a more elastic response, enduring stretch levels above $\lambda = 1.15$ with a more linear behavior. Stented D1 reveals a heterogeneous behavior longitudinally with tissue softening and stiffening, with mean stress favoring the latter. In addition, anisotropy is observed since the stented circumferential direction of D1 shows only softening. Both directions of D2 show isotropic tissue softening. D3 reveals anisotropy in both directions of non-stented tissue, but stiffening and isotropy are observed in the stented tissue. In the case of D4, the stented tissue does not show an aberrant response, but rather an early rupture of the non-stented tissue; possibly due to age-related tissue stiffening.

Stented tissue in group ii) is only stretched up to $\lambda = 1.10$ with a more nonlinear behavior and a more pronounced stiffness. Since the non-stented behavior reaches $\lambda = 1.20 - 1.25$ and statistically higher stresses, the influence of the stent seems to be larger in this group. Stented D5 reveals anisotropy between the two directions and follows a stiffer path with a shorter elastic phase compared to the non-stented behavior. Similar behavior is illustrated by D7 and D9, but circumferentially D7 does not show a different response. Based on age, D8 is highlighted as the stiffest tissue with some degree of anisotropy. The linear phase of the stented part is insignificant and it is noticeable that it withstands the highest stresses between the two groups. D6 in Fig. 3(iii) stands out as the youngest and the most elastic case. It withstands stresses in excess of 100 kPa and stretch levels in excess of 1.3, and the stented behavior exhibits anisotropy. The stress level is within the physiological range for healthy tissue, in agreement with the values reported in [16].

By comparing non-stented and stented tissues, the stress–stretch response of the stented region shows a stiffer behavior with an earlier entry in the nonlinear phase. The stented tissue shows a shorter stretch-based elastic phase, i.e., the first part of the curve, compared to the non-stented tissue, implying a loss of elastic fibers and it is consistent with [48]. In the interest of quantifying the nonlinear transition of the curve, we refer to the characterization of valuable parameters as described in Pokutta-Paskaleva et al. [49]. Although no discernible pattern is observed in either group, it is reasonable to conclude that the stent-graft affects the tissue with a tendency to stiffen it. Stented stress levels at maximum stretch vary and are not always lower than non-stented stresses. It is still unclear whether the reduced stress on the stented tissue is due to the stent-graft and/or the oversizing or other pathological reasons.

### 3.4. Global vs local behavior

Table 3 correlates the local and global effect of the stent on the aortic wall. In particular, it compares mean stress values at

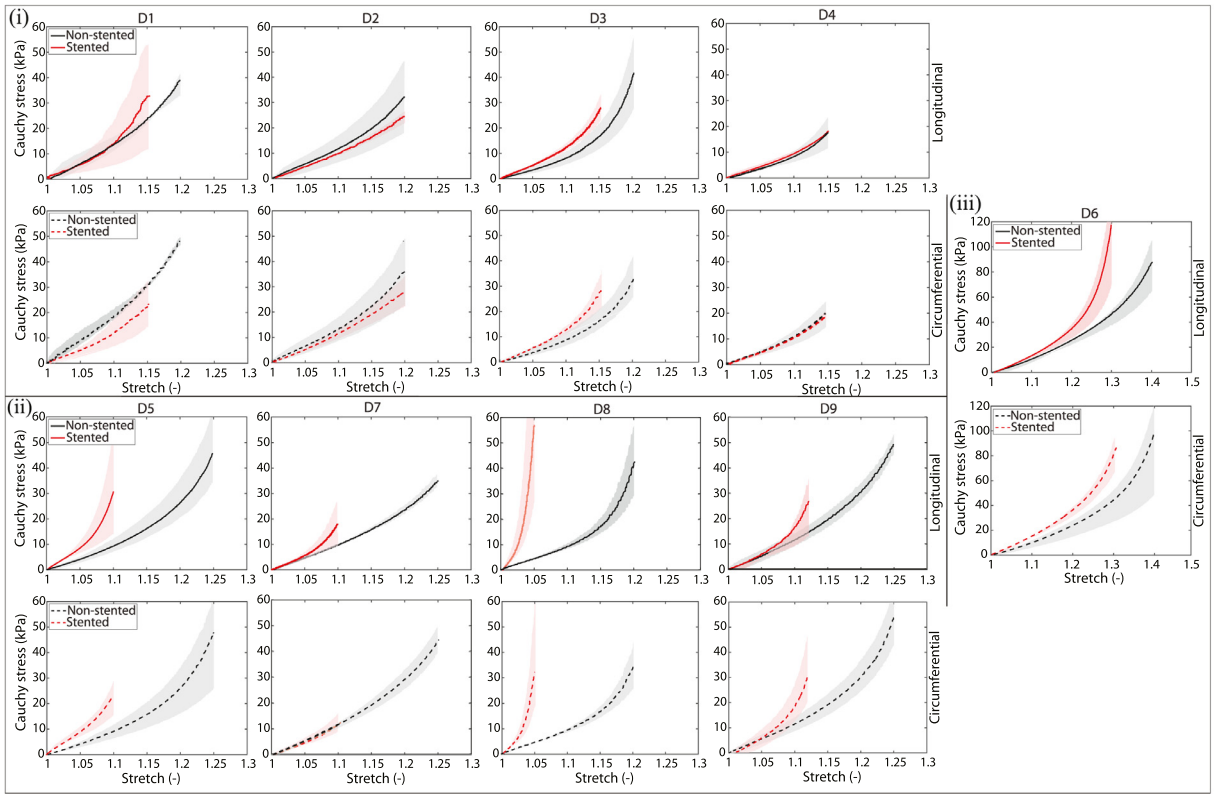


**Fig. 3.** Equibiaxial mean Cauchy stress–stretch responses between the proximal non-stented (black curves) and the proximal stented tissues (red curves) in the longitudinal direction (solid curves) and the circumferential direction (dashed curves) for all donors (D#). The semi-transparent areas show the standard deviation between the respective samples. The curves are grouped into (i) a higher stented elastic response and (ii) a lower stented elastic response, while D6 is an exception due to age and mechanical response, see (iii). (For interpretation of the references to colour in this figure legend, the reader is referred to the web version of this article.)

**Table 3**
Correlation of the proximal local vs global response of non-stented vs stented tissue with mean Cauchy stress at maximum and reference stretch level, the stented response of the tissue together with the loss of distensibility and the oversizing parameters.

| Donor Age | Condition (n) | $\sigma_{mean}$–$\lambda_{max}$ | | $\sigma_{mean}$–$\lambda_{ref}$ | | Local Response | | Global response | |
|---|---|---|---|---|---|---|---|---|---|
| (yrs) | | Long (kPa) | Circ (kPa) | Long/Circ (kPa) | $\lambda_{ref}$ (-) | Long (-) | Circ (-) | $D_{loss}$ (%) | Oversizing (%) |
| D1 60 | Non-stented (3) | 38.46 | 44.52 | 21.39/23.54 | 1.15 | - | - | - | - |
| | Stented (4) | 32.37 | 24.33 | 32.37/24.33 | 1.15 | Stiffening Softening | Softening | 25 | 15 |
| D2 56 | Non-stented (3) | 30.23 | 32.65 | 30.23/32.65 | 1.20 | - | - | - | - |
| | Stented (3) | 24.50 | 27.43 | 24.50/27.43 | 1.20 | Softening | Softening | 27 | 10 |
| D3 65 | Non-stented (4) | 41.08 | 31.09 | 15.79/15.31 | 1.15 | - | - | - | - |
| | Stented (5) | 29.14 | 28.57 | 29.14/28.57 | 1.15 | Stiffening | Stiffening | 69 | 25 |
| D4 81 | Non-stented (3) | 17.16 | 19.33 | 17.16/19.33 | 1.15 | - | - | - | - |
| | Stented (4) | 17.18 | 18.20 | 17.18/18.20 | 1.15 | Inconclusive | Inconclusive | 45 | 15 |
| D5 62 | Non-stented (4) | 45.87 | 47.77 | 8.83/8.14 | 1.10 | - | - | - | - |
| | Stented (6) | 31.16 | 22.54 | 31.16/22.54 | 1.10 | Stiffening | Stiffening | 88 | 20 |
| D6 38 | Non-stented (6) | 87.66 | 96.65 | 44.14/42.12 | 1.30 | - | - | - | - |
| | Stented (6) | 117.60 | 86.05 | 117.60/86.05 | 1.30 | Stiffening | Stiffening | 45 | 10 |
| D7 61 | Non-stented (5) | 21.38 | 23.32 | 11.78/12.48 | 1.10 | - | - | - | - |
| | Stented (4) | 17.88 | 12.56 | 17.88/12.56 | 1.10 | Stiffening | Inconclusive | 38 | 10 |
| D8 79 | Non-stented (4) | 42.46 | 34.67 | 4.13/4.15 | 1.05 | - | - | - | - |
| | Stented (6) | 56.72 | 32.02 | 56.72/32.02 | 1.05 | Stiffening | Stiffening | 57 | ≤10 |
| D9 62 | Non-stented (4) | 49.13 | 54.12 | 14.27/14.28 | 1.12 | - | - | - | - |
| | Stented (6) | 27.08 | 29.48 | 27.08/29.48 | 1.12 | Stiffening | Stiffening | 60 | 10 |

D = donor; $n$ = number of biaxial samples; $\sigma_{mean}$ = mean Cauchy stress; $\lambda_{max}$ = maximum stretch; $\lambda_{ref}$ = reference stretch; Long = longitudinal; Circ = circumferential; $D_{loss}$ = loss of distensibility

the maximum stretch level ($\sigma_{mean}$–$\lambda_{max}$), at the reference stretch level ($\sigma_{mean}$–$\lambda_{ref}$) and the stented tissue response for the longitudinal and circumferential directions. Other meaningful correlations consider stress-stretch behavior with local tissue response in both directions against the loss of distensibility ($D_{loss}$) and oversizing for each donor.

D1 and D2 are of similar age and are the only cases showing local softening. However, this contradicts the global behavior, which has the lowest $D_{loss}$ and is the least affected by oversizing. An oversizing of D1 with 15% shows anisotropy, local stretch of $\lambda_{max}$ = 1.15 and stresses of 32.37/24.33 kPa (long/circ). D2 with 10% oversizing does not deviate significantly for stresses (24.50/27.43 kPa) next to $\lambda_{max}$ = 1.20. D3 experienced the greatest oversizing with 25%, resulting in a large elastomechanical loss of 69% and local stiffening. However, the tissue response with stent showed isotropy with $\lambda_{max}$ = 1.15 and stresses similar to D1-D2, which

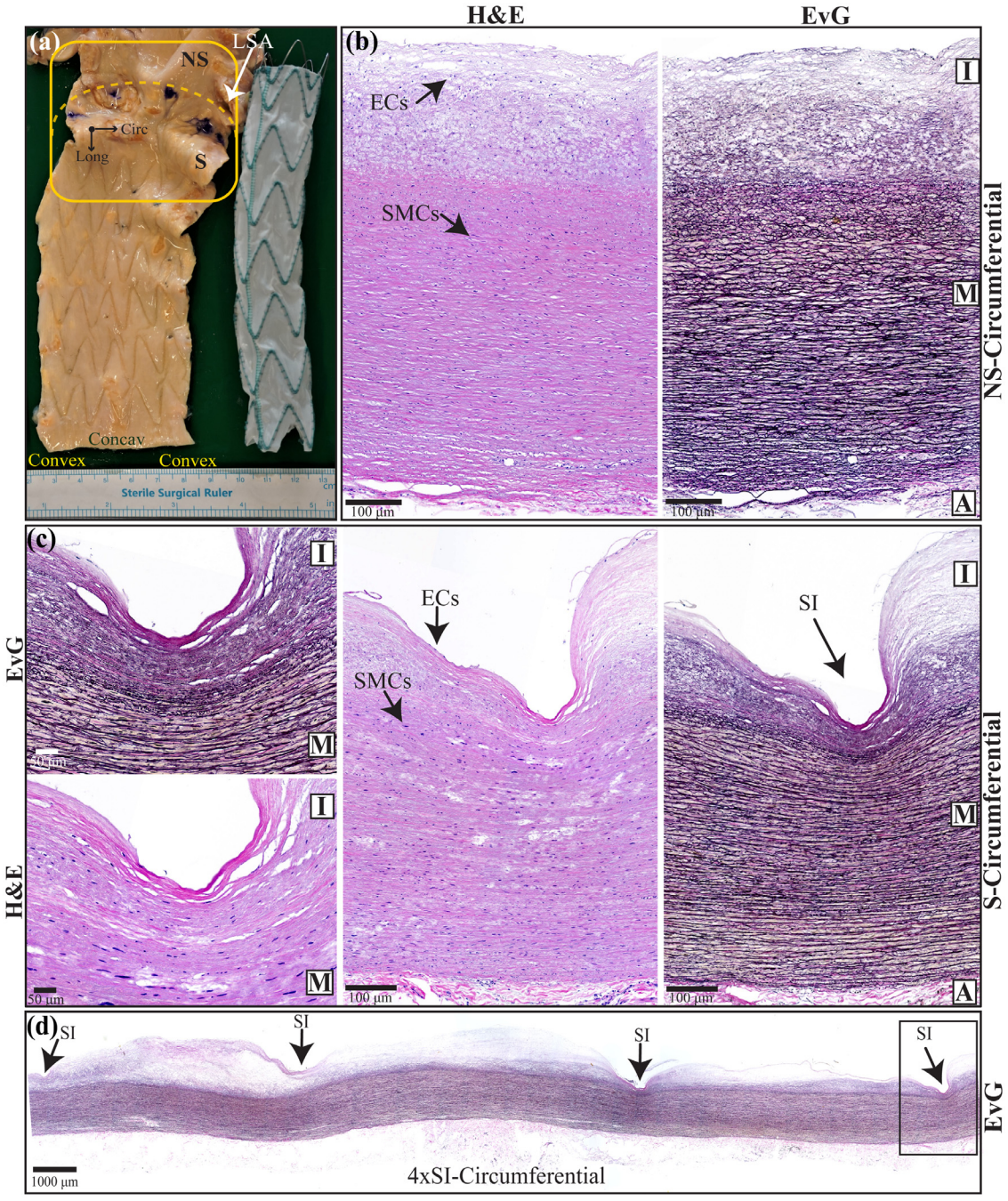


**Fig. 4.** Representative lumen strut-induced histological alterations after perfusion: (a) Dissected aorta (D3) shown along the convexity. After detachment of the stent graft, global strut patterns with an oversizing of 25% are visible. The yellow rectangle represents the proximal area, which is divided NS and S zones by a dashed curve. Black arrows point in the longitudinal (Long) and circumferential (Circ) directions. Distal from the LSA, tissue inks mark the location of the bare struts where the stent-graft was deployed. (b) Local NS wall (D10) with distinct intima (I), media (M), and adventitia (A) in the circumferential direction stained with H&E and EvG. The wall presents a healthy and physiological configuration with diffuse intimal hyperplasia. EC-SMCs cell nuclei appear dark blue and the ECM pink (H&E). Collagen fibers in I appear in purple color and elastic fibers in M in dark brown (EvG). (c) The strut-induced S-wall of 20% oversizing in the circumferential direction is illustrated with the three layers stained with H&E and EvG. SI-zoomed images on the left show a closer view of the SI region for two layers (I),(M). EC-SMCs appear to be viable despite *ex vivo* perfusion. SMCs have adapted to the new loading condition and appear stretched compared to the NS state. The SI compresses the I, delaminates the collagen and stretches the elastic fibers of the M (EvG). (d) A circumferential configuration in EvG identified with four consecutive SIs. A black rectangle shows the SI-wall analyzed in (c). NS = non-stented zone; S = stented zone; LSA = left subclavian artery; I = intima; M = media; A = adventitia; ECs = endothelial cells; SMCs = smooth muscle cells; H&E = hematoxylin and eosin; EvG = elastica van Gieson; SI = strut indentation. (For interpretation of the references to colour in this figure legend, the reader is referred to the web version of this article.)

were smaller and belong to the same age group. D4 endured stretches of 1.15, but the local response showed the least stress; with stent (17.18/18.20 kPa) and without stent (17.16/19.33 kPa). Low stresses and inconclusive trends between both directions of the stented tissue are justified by the donor's age (81), where stiffness might be innate. However, the post-stented $D_{loss}$ was significant (45%) due to oversizing of 15%.

D5 suffered the largest distensibility loss (88%) and was 20% oversized. This is also reflected locally in the mere stretch of $\lambda_{max} = 1.10$, which promotes tissue stiffening. In this case, D5

encountered a two-fold discrepancy: the compliance mismatch and the stent mismatch of the loading path compared to that without a stent. At $\lambda_{ref} = 1.10$, the mean stresses of the non-stented (8.83/8.18 kPa) deviate remarkably from the stented and anisotropic responses (31.16/22.54 kPa) outlining the stiffness in both stretch directions for the stented tissue. In contrast to all other cases, D6, as the youngest and most elastic case, demonstrates a two-fold increase in mean stresses for $\lambda_{max}$. At $\lambda_{ref} = 1.30$ endured stresses 44.14/42.12 kPa without stent and 117.60/86.05 kPa with stent, assuming a stiffened response. Oversizing by 10% showed compromised elasticity globally and tissue stiffening with some stent anisotropy locally. With an oversizing of 10%, D7 responded with losses of $D_{loss} = 38\%$. This is reflected in the stented loading path with low stresses and stretches of the local tissue with a slight longitudinal stiffening. The circumferential response of the stent appears to be inconclusive. D8 showed the stiffest response in the stented area of both groups with a stretch of only 1.05 along with the highest stented stresses (56.72/32.02 kPa) and an anisotropic trend. The effect of the $\leq 10\%$ oversizing is striking in the $D_{loss}$ and in the mechanical behavior when considering the non-stented tissue response. Finally, the stented response of D9 can be defined as isotropic, showed stiffening and a short elastic phase and endured lower stresses of 27.08/29.48 kPa against the non-stented tissue of 49.13/54.12 kPa at $\lambda_{max}$. The loss of elasticity is globally consistent ($D_{loss} = 60\%$) oversized with 10%.

Despite the limited cases, correlation based on age group ($56 - 65$ years old) with D1-D3, D5, D7, and D9 is permissible. By observing the non-stented paths, $\lambda_{max}$ reached 1.20 and beyond that (1.25) for D5, D7, and D9 with an elastic phase up to 1.15. Cauchy stresses for both directions varied $\sigma^{non-stented}_{min,max} \in [21.38, 49.13/23.32, 54.12]$ kPa. Stented loading pathways showed a shorter elastic phase and weaker responses with $\sigma^{stented}_{min,max} \in [17.88, 32.37/12.56, 32.02]$ kPa. With the exception of D2, whose non-stented tissue appears weaker and with stenting it shows tissue softening. In addition, the systolic displacement suffered notable losses in distensibility ranging from 25 to 69%, although the losses are not exclusively or directly related to the degree of oversizing.

Certain cases can be correlated with $\leq 10\%$ oversizing and with $\gg 10\%$ oversizing. At 10%, D2 and D6-D9 they manifest a considerable $D_{loss}$, although mere oversizing nevertheless has a controversial stent-induced elasticity where stiffness predominates. Local responses display strongly different stress values in both directions. Despite the usual sizing, the stented behavior of the tissue shows no pattern. For $\gg 10\%$ oversizing (D1 and D3-D5) it is unclear whether the oversizing itself has a direct impact on the tissue response as the responses are locally heterogeneous. $D_{loss}$ is not proportional to size increase, which is partially true of the global behavior. Nonetheless, losses ranged between 25 to 88%, confirming a compliance mismatch with arguable responses of tissue softening, stiffening, and inconclusive results.

### 3.5. Histology

A representative lumen topography of human tissue (D3, 25% of oversizing) after stent-graft detachment is shown in Fig. 4(a). Strut indentations (SIs) are distinguished by a 'zigzag' pattern circumferentially and expand repeatedly in the longitudinal direction. We consider the proximal location to be the area within the rounded rectangle where non-stented (NS) and stented (S) zones are separated. The position of the bare struts was color-coded to mark the start of the stent and to differentiate the NS and S zones. NS zone is adjacent to the bare struts, while the S zone is distal to the LSA and 'zigzags' to the first three struts including the bare struts. The histological protocol required fixation of the entire stented aorta (see Section 2.5). Therefore, the histological images in Fig. 4(b)-(d) refer to a separate case (D10, 20% of oversizing). Two representative samples of NS and S were chosen to demonstrate the effect of SI on the wall. Both samples were obtained in the circumferential direction as in the longitudinal orientation the indentations appeared to be less sharp in comparison. However, we believe this is due to the handling of the slices and not because the SI effect is reduced in that direction.

The histological evidence in Fig. 4(b) shows the distinguishable NS wall layers which appear to remain intact despite ex vivo perfusion. EvG staining reveals dense collagen fibers in purple in the thickened (diffusely hyperplastic) intima (I), while the dark brown elastic fibers in the media (M) appear wavy and in their physiological state. H&E staining was performed with dark blue for nuclei identification. ECs in the intima and SMCs in the media appear viable and in physiological numbers. The white 'empty' areas in the media were foamy histiocytes containing lipids that were dissolved during tissue dehydration.

In contrast, EvG on the S wall in Fig. 4(c) shows a strut-induced indentation that compresses the collagenous, diffusely hyperplastic intima onto the internal elastic membrane interface separating I and M. This effect propagates within the elastic fibers of the media, but the compression reduces towards the adventitia. Morphologically, the elastic fibers appear more linear but are not noticeably reduced after oversizing. They appear to be stretched, adjacent to the indentation, and moderately affected radially. It is very likely that this structural remodeling favors support against the strut by distributing the load. Notably, ECs of the S intima (H&E) maintain their physiological shape and appear to be viable despite long-term stress-based ex vivo perfusion and stenting. At a first glance, there is no major histopathological difference between the NS and S walls. However, when zooming into the I-M section in Fig. 4(c),(left) for both staining, the surrounding collagen fibers appear delaminated due to strut compression. This could be some form of local injury. In addition, the compression forces the media lamellae to stretch in a radial configuration, creating a 'boat-like' structural remodeling consistent with the strut-indented tissue in [50]. Between the lamellae, dark blue SMCs nuclei appear to maintain viability while being stretched in the adjacent region, suggesting *ex vivo* adaptation to SI loading. In Fig. 4(d), four consecutive SIs are observed in a longer EvG-stained circumferential segment. The SI wall in the black rectangle is the stented wall analyzed in 4(c). The two SIs on the left show a milder SI against the wall. Slight compression of the wall can be seen on the right SIs. Another finding concerns the collagen fibers of the intima in the strut-free area. It appears that the fabric of the graft does not affect mechanically the wall and therefore no deformation occurs. This is particularly evident in Fig. 4(d).

## 4. Discussion

TEVAR is a standard treatment technique for aortic pathology and has the highest survival rates among descending aorta treatments [51]. However, the early biomechanical impact of the stent-graft against the aortic wall remains uncertain. In this in vitro study, an MCL was employed to perfuse freshly isolated aortas before and after stenting under physiological conditions. It is natural to expect aortic stiffening due to stenting, however in the present study we quantified its magnitude at the proximal site. The severe global loss of elasticity extends toward the descending stented aorta and toward the non-stented but potentially affected aortic arch. It is noteworthy that the decrease in distensibility of the aorta after stenting in vitro is not time-dependent. The elastomechanical gap develops in the first few hours after implantation and remains as such. Based on this, we believe that this is an insight into the in vivo condition, where compliance is not influ-

enced over months, but the loss of compliance occurs in the first hours after implantation and might not change significantly over time. It should be noted that the findings of this study relate to the behavior of healthy aortas. Surgeons rarely stent non-pathological aortas whose distensibility is intact. By default, pathologic aortas show reduced distensibility because stiffness predominates as progression of pathology [52]. Therefore, it is expected that stenting of pathological aortas will have less compliance loss.

As a patient-specific approach, this study aims to understand how the aortic wall changes its elastomechanical behavior locally and globally after TEVAR. In this way, the outcomes of the pre- and post-stented experimental periods could have a more realistic impact. The presented investigation correlates the ex vivo compliance of stented aortas with respect to oversizing, the local biomechanical properties of non-stented and stented tissue, and the strut-induced histological changes in the aortic wall. To the best of our knowledge, no in vitro study has been performed on human tissue undergoing endograft repair and tracking the elastomechanical transition.

### 4.1. Compliance mismatch

Each aorta is unique in terms of viscoelasticity and the effects of stenting are different in each case. Arterial compliance is by definition pressure-dependent and here aortic perfusion was pressure-controlled. Thus, it can be stated that the area within the hysteresis loops describes the energy that can be stored during a cardiac cycle within the aortic wall, which has decreased significantly after implantation. The hysteresis loops in Fig. 2(b)-(d) are derived based on the approach in [15] to capture the elastomechanical gap that the stent-graft promotes as the lumen-wall interface. This gap is quite pronounced after implantation in most cases, regardless of age or oversizing. In addition, the compliance gap increase due to two other factors, namely the oversizing and the length of the stent-graft [35].

Oversizing more than 10%, as in D3-D5 cases, will result in a greater loss of elasticity. Notable is D6, age of 38, showing the highest elastic behavior among the cases of group ii) matched by age. However, the loss of distensibility (45%) is noticeable with a mere oversizing of 10%. It can be assumed that the greater the oversizing, the deeper the indentation within the medial layer and the greater the strut-induced local remodeling. In Fig. 4(b), an oversizing of 20% compresses the intima at the local area of indentation. Despite the intimal hyperplasia, the SI acts deeper in the medial area, where the lamellae are slightly compressed and moderately stretched. In the case of a thinner intima, it could be implied that the media, with its elastic fibers under maximum tension or partially torn, experiences a higher state of stretch, especially around the stent strut. In vivo this might trigger overexpression of collagen fibers and locally turn them into a stiffer area. It is noteworthy that the adjacent strut-free intimal area projects from highly to slightly affected tissue and further to non-affected tissue. In contrast, the medial fibers appear homogeneously stretched beyond the area of indentation. This was observed in [26] with oversized stent-grafts in porcine aortas in vivo and by yielding strut forces against porcine coronary arteries in vitro [50]. Here, the intact zone of the intima between the struts appears remarkably intact considering that it is covered by the stiff graft.

Equally important is length coverage of the descending aorta. D1 − 2 were implanted with a stent-graft length of 80 mm and the elastic gap was not as pronounced, the loops were compromised to some extent but retained their viscoelastic behavior. The coverage of ≥ 130 mm reduces aortic compliance by lowering $d_{\text{circ}}^{\max}$ closer to zero, consistent with [38], results in porcine tissue. Assuming that the permanent local fiber stretch of the medial layer extends and recurs at each SI circumferentially and along the stent-graft length in the longitudinal direction, this effect is uniform. This may indicate that the aorta is adopting the compliance of the stent-graft in the clinical setting and that is undermining the Windkessel effect, a flag for induced cardiovascular effects. At this point, it must be said that although we observe the $D_{\text{loss}}$ effect in different magnitudes, it cannot be clearly determined whether these losses are due to the implantation of the stent-graft or to the oversizing factor. Hence, there is uncertainty as to when the global drop in elasticity will become relevant to oversizing.

### 4.2. Global vs local response

Hysteresis loops from $p_{\text{aorta}}$–$d_{\text{circ}}$ outline the impairment of cyclic expandability after implantation of the stent-graft. The region of the loop describing the energy stored during expansion shrinks significantly in the S1-S4 measurements. The shape of the loops and the area within them vary from case to case due to the inherent mechanical properties of the wall. The interplay between the increase in the systolic $p_{\text{aorta}}^{\text{sys}}$ and the expansion of the $d_{\text{circ}}$ (i.e. the slope of the curve) is interesting. The systolic slope of the loops has shifted from an elastic, nonlinear slope to a stiffer, more 'linear' slope and more in the perpendicular direction. A representative elastic case of this behavior is D3 and a stiffer case is D5 (Fig. 2(c),(d)). The stiffness of the aorta is also reflected in the diastolic path of the curve. For example, the non-stented D2-D3, D6-D7 and D9 provide a smooth, nonlinear transition from systole to diastole, i.e. the pressure decrease is followed by a proportionate distensible decrease. D1 and D4-D5 as stiffer cases, this effect is heterochronous and the diastolic curve is vertical. Stented periods adopt the delayed behavior regardless of the non-stented elastic behavior and age, and may be related to global stiffness. Based on the above, we can conclude that the cyclic expansion is constricted after implantation and the stored amount of liquid (i.e., blood in vivo) is reduced during systole, disrupting the diastolic perfusion. These manifestations relate to the proximal site but are also very likely responsible for the descending stented aorta. Physically, at least a constricted cyclic expansion was observed during the experiments.

Circumferential and longitudinal stresses stretched biaxially appear to plateau at 60 kPa, with the exception of D6, which is considered an age outlier. As demonstrated in [16], the physiological stresses of non-diseased tissues exceed 100 kPa. This lower threshold here shares the behavior without a stent and is caused by early rupture of the hooks under loading in the biaxial setup and not rupture of the tissue. Nonetheless, one could extrapolate the nonlinear feature of the stress-stretch response and estimate it beyond the measured range. The tissue responses with stents reach a lower stress threshold, with the exception of D6 (not comparable) and D8 (< 10% oversizing). Local injury to collagen and/or elastin fibers may occur due to SI compared to non-stented tissue; beyond the obvious delamination. EvG staining of stented tissue shows a conditioned media with fiber pre-stretching after SI. Subsequent equibiaxial stretch can start from this conditioned pre-stretched state and overstretches the fibers with a tendency to tear. Therefore, the maximum sustained stretch level before fiber rupture occurs earlier. This can affect both collagen and elastin fibers as the mechanical curves show different responses and no pattern. The local stress-stretch response of the stented area agrees with the global observations and proves the transition to aortic stiffening. Circumferential global compliance and local stretches almost always lose their initial non-stented behavior and result in lower stresses once they are stented. Whether the medial fiber pre-stretching of the stented samples occurs at the moment of deployment or during dynamic perfusion of the overstretched aortic wall is still controversial.

### 4.3. Histology

Histological evidence in the circumferential direction illustrates permanent stretching of the medial layer in the presence of a fibrotic intima. Collagen fibers appear compressed and elastic fibers stretched. The stiffening behavior could be due to a higher stent-induced elastin pre-stretch and an earlier maximal elongation of the collagen compared to the non-stented, whose aortic wall is not pre-stretched. Based on our histological examinations, neither an elastin nor a collagen fiber rupture was detectable. Despite this, stented mechanical responses have been rendered stiffer, allowing us to assume some loss of elastic fibers in the media. Clinically, the stretching of fibers or possibly overstretching in a non-fibrotic intima and/or more oversizing can trigger a cascade of events. The SI is perceived locally as damage and could mechanotransduce SMCs to differentiate from a contractile to a synthetic phenotype [25]. Synthetic SMCs would migrate, proliferate, and produce ECM components to help the injured tissue wall. The known disadvantages of this cascaded crosstalk are the expression of the MMP2/9s proteases to target and fragment elastin and that elastin expression is saturated early in life. The elastin content in the medial layer progressively decreases while SMCs would reach a state of collagen expression [47]. Continued collagen deposition due to permanent and cyclic overstretching and elastin fragmentation due to the synthetic phenotype will create an even stiffer aorta. For the above reasons, and if these local changes spread globally, the role of compliance can be further reduced [13,20,25].

The oversizing of 20% compressed the dense collagen fibers of the thick intima and the strut-induced loading caused collagen fibers to delaminate in the area surrounding the SI. Medial elastic fibers are affected moderately within the physiological range. These fibers appear more linear in the stented area, compared to the NS which are wavier, similar to the in vivo physiological fiber orientation under systolic pressure. Cellular content maintains its physiological state despite the indentation but also shows a feature of mechano-adaptation induced during ex vivo perfusion in the MCL. Ex vivo perfusion benefits from the bradytrophic aorta being resistant to cold ischemic periods. This could justify why ECs and SMCs appear viable in the intima without significant loss of cellular contents in the media. Postmortem tissue is reported to retain its cellular contents for up to 72 hours after tissue recovery [53,54]. The results of this study indicate that variations in cold ischemic times do not significantly affect tissue integrity and behavior. Therefore, the methods addressed here provide a friendly environment for evaluating human tissue. Importantly, histological evidence of the stented tissue shows wall remodeling without noticeable injuries in the media or local loss of elastic fibers. However, this does not exclude that some elastic fibers could have been disrupted by oversizing, as shown by the stiffer stress-stretch response.

The medial stretching fades towards the adventitia where it stops. Aortic wall remodeling indicates that vessel stretching due to stenting through the adventitia stops at a certain point and the adventitia becomes very stiff. This could be an explanation for the global loss of compliance in the stenting period. The stretched configuration with stent resembles the physiological non-stented wall configuration at systole. The permanent stretching caused by oversizing prevents the dampening of the systolic wave and the transition to diastole. Under this premise, less energy can be stored and the smaller area of the hysteresis loops can be justified. In addition, the permanent stented wall combined with cyclic systolic pressure increases the possibility of localized fiber rupture.

Since the findings are not 'textbook-like' it is difficult to argue whether strut-induced remodeling masks local damage and whether oversizing plays a role. Therefore, we can only provide an estimate based on the previous analysis and histological observations. A viscoelastic effect of the lumen wall was observed during detachment of the stent-graft. Locally indented tissue was restored after a few hours and the SI pattern disappeared. This has been observed in all degrees of oversizing, which is a sign of viscoelasticity and an indicator that the aortic wall can artificially undergo radial overstretching without major wall damage. Such behavior could indicate that the probability of strut-induced damage remains low. This is consistent with the histological results, which show no obvious mechanical injury to the wall layers. However, the present histological analysis cannot quantify damage (i.e. collagen rupture) and it is uncertain whether it occurred outside of the visible spectrum. As an alternative proposal and for future reference, a precise hybrid peptide mechanism can be used to bind to the denatured collagen, which would return a quantified fluorescent signal of the ruptured collagen through the wall [55].

### 4.4. Clinical setting

Thoracic compliance is a major contributor to overall aortic compliance. Implanting a stiffer stent-graft increases the stiffness and impairs aortic compliance. Long-term decreased aortic compliance occurs as a silent deleterious effect. Due to the undamped pressure, the aortic vessel experiences progressively modified wave reflections, which trigger proximal vascular effects [9]. Some loss of compliance can alter the ventricular-aortic coupling critical to aortic mechanics and may lead to a cascade of adverse (cardio)vascular events: increase of afterload, elevated PWV, and subsequently early arrival of systolic wave reflections. As a consequence, central systolic pressure (hypertensive) increases and diastolic pressure decreases resulting in an increase in afterload and reduced perfusion of the coronary arteries [56,57]. It is strongly associated with the loss of the Windkessel effect, which increases the ventricular workload and eventually induces adaptive hypertrophy [9,57]. Other potential adverse events caused by impaired coupling and supraphysiological loading include aortic valve dysfunction due to annular dilation and progressive aortic regurgitation [56].

In order to prevent misinterpretations, the authors do not intend to neglect the medical importance of endovascular stents, which have improved the quality of life in recent decades. It is rather a combination of findings to optimize vascular prostheses. In the present in vitro environment, the elastomechanical behavior of the proximal aorta ex vivo was impaired, independent of the degree of oversizing and the elasticity group, confirming the compliance mismatch. However, global, local, and histological evidence do not make the stent-graft a disadvantage. Correlations of shared oversize or age group indicate the challenge of extracting a response pattern between different cases. Factors other than the stent-graft itself that reduce tissue elasticity include the deployment site, length of coverage of the aorta, and oversizing. Against this background, it becomes even clearer that each case should be treated individually.

The mechanisms by which the implantation of the stent-graft leads to these vascular complications and whether they are clinically reversible are still unclear. Their reduction can be achieved by creating patient-specific, custom-made grafts with more compliant materials in the preoperative setting in consultation with clinicians. Interventionists rarely focus on the biomechanical and histological changes associated with ECM because they are clinically unavailable. Rather, they focus on the morphological adaptation of the stent-graft to the aortic wall despite the occurrence of the above effects. The experimental documentation of the biomechanical behavior and the wall alterations correlated with size variations after implantation are of importance. This proposition must be substantiated by clinical trials correlating patient-specific and

ECG-triggered sizing, taking into account trials on stent-induced histological alterations.

In clinical routine, CT is not ECG-triggered and stent-graft size is estimated from an arbitrary snapshot of the cardiac cycle, while preliminary diastolic-systolic diameter configurations are neglected. In chronic aneurysms and dissections, a CT scan is more likely to capture the sealing zone in diastole because it accounts for the longest part of the cycle. Clinically, an oversizing of 10 – 20% is targeted, but based on a diastolic snapshot where the diameter is smallest, the stent-graft may be undersized. Hence, endoleaks and stent-graft migration lurk. We believe that oversizing by 10 – 20% [5,23,58] may improve patient outcomes by accounting for: (i) ECG-triggered patient-specific diameter to compensate for the radial expansion of the stent-graft and the stretched contractile wall at systole [5], (ii) age of the patient; younger subjects have higher compliance than older subjects who are atherosclerotic, and the increased stiffness is congenital [5,15] and (iii) location of implantation; aortic compliance is greater proximally due to its high content of elastin, which decreases distally. Conversely, the collagen content is lower proximally and higher distally [6]. A patient-specific diagnosis, considering the above points and understanding the interaction between the stent-graft and the aortic wall, could lead to more appropriate sizing decisions and potentially prevent post-operative complications.

### 4.5. Future aspects

To better understand the role of oversizing, it is necessary to replicate the current findings and categorize stented aortas into oversizing groups. Furthermore, it is observed that the influence of the stent-graft on the elastomechanical behavior was transcribed within the first few hours. Therefore, follow-up studies will decrease perfusion time, with the potential benefit of preserving tissue integrity for post-processing. As a consequence, mechanical responses could be less affected. The current findings relate to the physiological scenario of the healthy state. Perfusion under the hypertensive scenario would be of interest to compare results between scenarios.

### 4.6. Limitations

It should be noted that inherent limitations such as connective tissue disorders or areas of atherosclerosis that could not be excluded from perfusion may have confounded our results. The orientation of the aortic arch is mirrored. Age-related atherosclerotic tissue was excluded from the mechanical assessment which limited the sample size. The stress-stretch responses between the non-stented and the stented tissue could have been affected by the positional difference of the samples. The TEVAR procedure was performed outside of the loop and in non-pressurized tissue to ensure the stent was deployed properly. ODs were measured with a digital caliper at constant mean pressure. In contrast to the clinical setting, aortic oversizing was random and based on available stent-graft sizes. Pressure measurements were not recorded directly in the lumen. Dynamic elasticity was not measured after stent removal because it remains a challenge to withdraw the stent-graft without dissecting the aorta and keeping the lumen wall intact. During the cyclic loading, the MCL captured the passive structural and mechanical alterations. Actual cell-mediated ECM changes within the wall could not be detected. A histological comparison between the donors was not possible with the current protocol.

## 5. Conclusion

For the first time, dynamic perfusion of explanted human thoracic aortas that underwent TEVAR in vitro demonstrated early stiffening of the aortic tissue in the post-stented period. Ex vivo loss of cyclic compliance describes the compliance mismatch between the stent-graft and the aortic wall. Despite the mismatch and oversizing, neither stent-induced injury nor a tendency for tissue softening of the stented wall was observed. Clinically, local and global stent-induced manifestations are challenging. The under-representation of biomechanical and histological properties of the aortic tissue makes the present work of high relevance. Comparisons between non-stented and stented human tissue can provide new insights into the interaction between the endograft and the aortic wall, refine stent-graft design and optimize quality of life after TEVAR. Therefore, extensive clinical–experimental studies to further assist in the development of super-adaptable endografts with natural compliance are crucial.

## Declaration of Competing Interest

The authors declare that they have no known competing financial interests or personal relationships that could have appeared to influence the work reported in this paper.

## Acknowledgement

We would like to acknowledge the valuable contribution of Professor Rupert Portugaller, MD, from the Division of Neuroradiology, Vascular and Interventional Radiology. We would like to thank JOTEC GmbH for providing the stent-grafts during this study.

## References

[1] J.A. Elefteriades, Thoracic aortic aneurysm: reading the enemy's playbook, Curr. Probl. Cardiol. 33 (5) (2008) 203–277.
[2] M. Grabenwöger, F. Alfonso, J. Bachet, R. Bonser, M. Czerny, H. Eggebrecht, A. Evangelista, R. Fattori, H. Jakob, L. Lönn, C.A. Nienaber, G. Rocchi, H. Rousseau, M. Thompson, E. Weigang, R. Erbel, Thoracic endovascular aortic repair (TEVAR) for the treatment of aortic diseases: a position statement from the european association for cardio-thoracic surgery (EACTS) and the european society of cardiology (ESC), in collaboration with the european association of percutaneous cardiovascular interventions (EAPCI), Eur. Heart J. 33 (13) (2012) 1558–1563.
[3] V. Riambau, D. Böckler, J. Brunkwall, P. Cao, R. Chiesa, G. Coppi, M. Czerny, G. Fraedrich, S. Haulon, M. Jacobs, M.L. Lachat, F.L. Moll, C. Setacci, P.R. Taylor, M. Thompson, S. Trimarchi, H.J. Verhagen, E.L. Verhoeven, E.G. Committee, P. Kolh, G.J. de Borst, N. Chakfé, E.S. Debus, R.J. Hinchliffe, S. Kakkos, I. Koncar, J.S. Lindholt, M. Vega de Ceniga, F. Vermassen, F. Verzini, P. Document Reviewers Kolh, J.H. Black 3rd, R. Busund, M. Björck, M. Dake, F. Dick, H. Eggebrecht, A. Evangelista, M. Grabenwöger, R. Milner, A.R. Naylor, J.-B. Ricco, H. Rousseau, J. Schmidli, Editor's choice–management of descending thoracic aorta diseases: clinical practice guidelines of the european society for vascular surgery (ESVS), Eur. J. Vasc. Surg. 53 (1) (2017) 4–52.
[4] S.W. Chen, K.B. Lee, M.A. Napolitano, A.E. Murillo-Berlioz, A.P. Sattah, S. Sarin, G. Trachiotis, Complications and management of the thoracic endovascular aortic repair, Aorta 8 (03) (2020) 049–058.
[5] J. Concannon, K. Moerman, N. Hynes, S. Sultan, J. McGarry, Influence of shape-memory stent grafts on local aortic compliance, Biomech. Model. Mechanobiol. 20 (6) (2021) 2373–2392.
[6] J. Concannon, P. Dockery, A. Black, S. Sultan, N. Hynes, P. McHugh, K. Moerman, J. McGarry, Quantification of the regional bioarchitecture in the human aorta, J. Anat. 236 (1) (2020) 142–155.
[7] E.B. Diethrich, Endovascular or open treatment of aortic coarctation (typical and atypical), in: Thoraco-Abdominal Aorta: Surgical and Anesthetic Management, in: Chiesa, R., Melissano, G., Zangrillo, A. (Eds), Springer, Milano, 2011, pp. 541–553.
[8] N. Tai, H. Salacinski, A. Edwards, G. Hamilton, A. Seifalian, Compliance properties of conduits used in vascular reconstruction, Journal of British Surgery 87 (11) (2000) 1516–1524.
[9] C. Spadaccio, F. Nappi, N. Al-Attar, F.W. Sutherland, C. Acar, A. Nenna, M. Trombetta, M. Chello, A. Rainer, Old myths, new concerns: the long-term effects of ascending aorta replacement with dacron grafts. not all that glitters is gold, J. Cardiovasc. Transl. Res. 9 (4) (2016) 334–342.

[10] G.E. McVeigh, A.J. Bank, J.N. Cohn, Arterial compliance, in: Cardiovascular Medicine, in: J. T. Willerson and J. N. Cohn, H. J. J. Wellens and D. R. Holmes (Eds), Springer, 2007, pp. 1811–1831.
[11] A. Valentin, J.D. Humphrey, G.A. Holzapfel, A multi-layered computational model of coupled elastin degradation, vasoactive dysfunction, and collagenous stiffening in aortic aging, Ann. Biomed. Eng. 39 (7) (2011) 2027–2045.
[12] S. Jana, M. Hu, M. Shen, Z. Kassiri, Extracellular matrix, regional heterogeneity of the aorta, and aortic aneurysm, Experimental & Molecular Medicine 51 (12) (2019) 1–15.
[13] P. Lacolley, V. Regnault, P. Segers, S. Laurent, Vascular smooth muscle cells and arterial stiffening: relevance in development, aging, and disease, Physiol. Rev. 97 (4) (2017) 1555–1617.
[14] T. Mimler, C. Nebert, E. Eichmair, B. Winter, T. Aschacher, M.-E. Stelzmueller, M. Andreas, M. Ehrlich, G. Laufer, B. Messner, Extracellular matrix in ascending aortic aneurysms and dissections–what we learn from decellularization and scanning electron microscopy, PLoS ONE 14 (3) (2019) e0213794.
[15] M. Amabili, P. Balasubramanian, I. Bozzo, I.D. Breslavsky, G. Ferrari, G. Franchini, F. Giovanniello, C. Pogue, Nonlinear dynamics of human aortas for material characterization, Phys. Rev. X 10 (1) (2020) 011015.
[16] M. Jadidi, M. Habibnezhad, E. Anttila, K. Maleckis, A. Desyatova, J. MacTaggart, A. Kamenskiy, Mechanical and structural changes in human thoracic aortas with age, Acta Biomater. 103 (2020) 172–188.
[17] Y. Nakashima, Y.-X. Chen, N. Kinukawa, K. Sueishi, Distributions of diffuse intimal thickening in human arteries: preferential expression in atherosclerosis-prone arteries from an early age, Virchows Archiv 441 (3) (2002) 279–288.
[18] D. Lu, G.S. Kassab, Role of shear stress and stretch in vascular mechanobiology, Journal of the Royal Society Interface 8 (63) (2011) 1379–1385.
[19] N. Bogunovic, J.P. Meekel, D. Micha, J.D. Blankensteijn, P.L. Hordijk, K.K. Yeung, Impaired smooth muscle cell contractility as a novel concept of abdominal aortic aneurysm pathophysiology, Sci. Rep. 9 (1) (2019) 1–14.
[20] J.D. Humphrey, M.A. Schwartz, G. Tellides, D.M. Milewicz, Role of mechanotransduction in vascular biology: focus on thoracic aortic aneurysms and dissections, Circ. Res. 116 (8) (2015) 1448–1461.
[21] S. Sherifova, G.A. Holzapfel, Biochemomechanics of the thoracic aorta in health and disease, Progress in Biomedical Engineering 2 (3) (2020) 032002.
[22] I. Mohan, R. Laheij, P. Harris, Risk factors for endoleak and the evidence for stent-graft oversizing in patients undergoing endovascular aneurysm repair, European Journal of Vascular and Endovascular Surgery 21 (4) (2001) 344–349.
[23] J. van Prehn, F.J. Schlösser, B.E. Muhs, H.J. Verhagen, F.L. Moll, J.A. van Herwaarden, Oversizing of aortic stent grafts for abdominal aneurysm repair: a systematic review of the benefits and risks, European Journal of Vascular and Endovascular Surgery 38 (1) (2009) 42–53.
[24] C. Ioannou, N. Stergiopulos, A. Katsamouris, I. Startchik, A. Kalangos, M. Licker, N. Westerhof, D. Morel, Hemodynamics induced after acute reduction of proximal thoracic aorta compliance, European Journal of Vascular and Endovascular Surgery 26 (2) (2003) 195–204.
[25] D. Dajnowiec, B.L. Langille, Arterial adaptations to chronic changes in haemodynamic function: coupling vasomotor tone to structural remodelling, Clin. Sci. 113 (1) (2007) 15–23.
[26] I.R. Sincos, E.S. da Silva, S.Q. Belczak, A.P.W.B. Sincos, M. de Lourdes Higuchi, V. Gornati, J.P. Otoch, R. Aun, Histologic analysis of stent graft oversizing in the thoracic aorta, J. Vasc. Surg. 58 (6) (2013) 1644–1651.
[27] J.D. Humphrey, G.A. Holzapfel, Mechanics, mechanobiology, and modeling of human abdominal aorta and aneurysms, J. Biomech. 45 (5) (2012) 805–814.
[28] J.C. Kohn, M.C. Lampi, C.A. Reinhart-King, Age-related vascular stiffening: causes and consequences, Front. Genet. 6 (2015) 112.
[29] E. Agrafiotis, M.A. Geith, M.A. Golkani, V. Hergesell, G. Sommer, S. Spiliopoulos, G.A. Holzapfel, An active approach of pressure waveform matching for stress-based testing of arteries, Artif. Organs (2021).
[30] P. Lantelme, A. Dzudie, H. Milon, G. Bricca, L. Legedz, J.-M. Chevalier, P. Feugier, Effect of abdominal aortic grafts on aortic stiffness and central hemodynamics, J. Hypertens. 27 (6) (2009) 1268–1276.
[31] V.D. Tzilalis, D. Kamvysis, P. Panagou, I. Kaskarelis, M.K. Lazarides, T. Perdikides, P. Prassopoulos, H. Boudoulas, Increased pulse wave velocity and arterial hypertension in young patients with thoracic aortic endografts, Ann. Vasc. Surg. 26 (4) (2012) 462–467.
[32] K.G. Moulakakis, S.N. Mylonas, J. Kakisis, N.P. Kadoglou, I. Papadakis, G.S. Sfyroeras, C.C. Antonopoulos, G. Mantas, I. Ikonomidis, C.D. Liapis, Arterial stiffness alterations and inflammatory response following endovascular aortic repair, Aorta 3 (02) (2015) 75–80.
[33] A. Youssef, I. Kalaja, U. Alkomi, T. Abt, R.-T. Hoffmann, C. Reeps, N. Weiss, H.K. Lackner, A. Mahlmann, Aortic stiffness and related complications after endovascular repair of blunt thoracic aortic injury in young patients, VASA 49 (4) (2020) 295–300.
[34] Y. Takeda, Y. Sakata, T. Ohtani, S. Tamaki, Y. Omori, Y. Tsukamoto, Y. Aizawa, K. Shimamura, Y. Shirakawa, T. Kuratani, Y. Sawa, K. Yamamoto, T. Mano, I. Kormuro, Endovascular aortic repair increases vascular stiffness and alters cardiac structure and function, Circulation Journal (2013) CJ–13.
[35] H.W. De Beaufort, M. Conti, A.V. Kamman, F.J. Nauta, E. Lanzarone, F.L. Moll, J.A. Van Herwaarden, F. Auricchio, S. Trimarchi, Stent-graft deployment increases aortic stiffness in an ex vivo porcine model, Ann. Vasc. Surg. 43 (2017) 302–308.
[36] H.W. De Beaufort, M. Coda, M. Conti, T.M. Van Bakel, F.J. Nauta, E. Lanzarone, F.L. Moll, J.A. Van Herwaarden, F. Auricchio, S. Trimarchi, Changes in aortic pulse wave velocity of four thoracic aortic stent grafts in an ex vivo porcine model, PLoS ONE 12 (10) (2017) e0186080.
[37] F.J. Nauta, M. Conti, S. Marconi, A.V. Kamman, G. Alaimo, S. Morganti, A. Ferrara, J.A. Van Herwaarden, F.L. Moll, F. Auricchio, S. Trimarchi, An experimental investigation of the impact of thoracic endovascular aortic repair on longitudinal strain, European Journal of Cardio-Thoracic Surgery 50 (5) (2016) 955–961.
[38] F.J. Nauta, H.W. de Beaufort, M. Conti, S. Marconi, A.V. Kamman, A. Ferrara, J.A. van Herwaarden, F.L. Moll, F. Auricchio, S. Trimarchi, Impact of thoracic endovascular aortic repair on radial strain in an ex vivo porcine model, European Journal of Cardio-Thoracic Surgery 51 (4) (2017) 783–789.
[39] G. Ferrari, P. Balasubramanian, E. Tubaldi, F. Giovanniello, M. Amabili, Experiments on dynamic behaviour of a dacron aortic graft in a mock circulatory loop, J. Biomech. 86 (2019) 132–140.
[40] M. Amabili, P. Balasubramanian, G. Ferrari, G. Franchini, F. Giovanniello, E. Tubaldi, Identification of viscoelastic properties of dacron aortic grafts subjected to physiological pulsatile flow, J. Mech. Behav. Biomed. Mater. 110 (2020) 103804.
[41] S. Boës, G. Ochsner, R. Amacher, A. Petrou, M. Meboldt, M. Schmid Daners, Control of the fluid viscosity in a mock circulation, Artif Organs 42 (1) (2018) 68–77.
[42] R.H. Mohiaddin, P.J. Kilner, S. Rees, D.B. Longmore, Magnetic resonance volume flow and jet velocity mapping in aortic coarctation, J. Am. Coll. Cardiol. 22 (5) (1993) 1515–1521.
[43] Jotec GmbH, E-vita Thoracic 3G Stent Graft System, Instructions for Use, Hechingen, Germany, 2015.
[44] B. Zipfel, The Jotec Devices, in: R. Chiesa, G. Melissano, A. Zangrillo (Eds.), Thoraco-Abdominal Aorta: Surgical and Anesthetic Management, Springer Milan, Milano, 2011, pp. 705–717.
[45] G. Sommer, D.C. Haspinger, M. Andrä, M. Sacherer, C. Viertler, P. Regitnig, G.A. Holzapfel, Quantification of shear deformations and corresponding stresses in the biaxially tested human myocardium, Ann. Biomed. Eng. 43 (10) (2015) 2334–2348.
[46] J. Schindelin, I. Arganda-Carreras, E. Frise, V. Kaynig, M. Longair, T. Pietzsch, S. Preibisch, C. Rueden, S. Saalfeld, B. Schmid, J.-Y. Tinevez, D.J. White, V. Hartenstein, K. Eliceiri, P. Tomancak, A. Cardona, Fiji: an open-source platform for biological-image analysis, Nat. Methods 9 (7) (2012) 676–682.
[47] C.-J. Lin, A.J. Cocciolone, J.E. Wagenseil, Elastin, arterial mechanics, and stenosis, American Journal of Physiology-Cell Physiology 322 (5) (2022) C875–C886.
[48] H. Weisbecker, C. Viertler, D.M. Pierce, G.A. Holzapfel, The role of elastin and collagen in the softening behavior of the human thoracic aortic media, J. Biomech. 46 (11) (2013) 1859–1865.
[49] A. Pokutta-Paskaleva, F. Sulejmani, M. DelRocini, W. Sun, Comparative mechanical, morphological, and microstructural characterization of porcine mitral and tricuspid leaflets and chordae tendineae, Acta Biomater. 85 (2019) 241–252.
[50] M.A. Geith, L. Nothdurfter, M. Heiml, E. Agrafiotis, M. Gruber, G. Sommer, T.G. Schratzenstaller, G.A. Holzapfel, Quantifying stent-induced damage in coronary arteries by investigating mechanical and structural alterations, Acta Biomater 116 (2020) 285–301.
[51] A.M. Booher, E.M. Isselbacher, C.A. Nienaber, S. Trimarchi, A. Evangelista, D.G. Montgomery, J.B. Froehlich, M.P. Ehrlich, J.K. Oh, J.L. Januzzi, P. O'Gara, M. Thoralf, K.M. Harris, E. Bossone, R.E. Pyeritz, K.A. Eagle, m. Investigators, The IRAD classification system for characterizing survival after aortic dissection, Am. J. Med. 126 (8) (2013) 730–e19–24.
[52] P. Panpho, Y. Yang, H.A. Davies, O. Nawaytou, A. Harky, F. Torella, M. Field, J. Madine, R. Akhtar, Time-dependent mechanical behaviour of the aortic chronic dissection flap, Interact. Cardiovasc. Thorac. Surg. 34 (5) (2022) 892–901.
[53] M.K. Shikh Alsook, A. Gabriel, J. Piret, O. Waroux, C. Tonus, D. Connan, E. Baise, N. Antoine, Tissues from equine cadaver ligaments up to 72 hours of post–mortem: a promising reservoir of stem cells, Stem Cell Research & Therapy 6 (1) (2015) 1–10.
[54] F.E. Smit, D. Bester, J.J. van den Heever, F. Schlegel, L. Botes, P.M. Dohmen, Does prolonged post-mortem cold ischemic harvesting time influence cryopreserved pulmonary homograft tissue integrity? Cell Tissue Bank 16 (4) (2015) 531–544.
[55] J.L. Zitnay, Y. Li, Z. Qin, B.H. San, B. Depalle, S.P. Reese, M.J. Buehler, S.M. Yu, J.A. Weiss, Molecular level detection and localization of mechanical damage in collagen enabled by collagen hybridizing peptides, Nat. Commun. 8 (1) (2017) 1–12.
[56] C. Vlachopoulos, K. Aznaouridis, C. Stefanadis, Prediction of cardiovascular events and all-cause mortality with arterial stiffness: a systematic review and meta-analysis, J. Am. Coll. Cardiol. 55 (13) (2010) 1318–1327.
[57] I. Ikonomidis, V. Aboyans, J. Blacher, M. Brodmann, D.L. Brutsaert, J.A. Chirinos, M. De Carlo, V. Delgado, P. Lancellotti, J. Lekakis, D. Mohty, P. Nihoyannopoulos, J. Parissis, D. Rizzoni, F. Ruschitzka, P. Seferovic, E. Stabile, D. Tousoulis, D. Vinereanu, C. Vlachopoulos, D. Vlastos, P. Xaplanteris, R. Zimlichman, M. Metra, The role of ventricular–arterial coupling in cardiac disease and heart failure: assessment, clinical implications and therapeutic interventions. a consensus document of the european society of cardiology working group on aorta & peripheral vascular diseases, european association of cardiovascular imaging, and heart failure association, Eur. J. Heart Fail. 21 (4) (2019) 402–424.
[58] K.P. Donas, M.V. Usai, G.T. Taneva, F.J. Criado, G.B. Torsello, P. Kubilis, S. Scali, F.J. Veith, Impact of aortic stent-graft oversizing on outcomes of the chimney endovascular technique based on a new analysis of the pericles registry, Vascular 27 (2) (2019) 175–180.